

Nano-engineered non-uniform strain in graphene

M. Neek-Amal^{1,2}, L. Covaci² and F. M. Peeters²

¹*Department of Physics, Shahid Rajaei University, Lavizan, Tehran 16785-136, Iran.*

²*Departement Fysica, Universiteit Antwerpen, Groenenborgerlaan 171, B-2020 Antwerpen, Belgium.*

(Dated: July 30, 2018)

Recent experiments showed that non-uniform strain can be produced by depositing graphene over pillars. We employed atomistic calculations to study the non-uniform strain and the induced pseudo-magnetic field up to 5000 Tesla in graphene on top of nano-pillars. By decreasing the distance between the nano-pillars a complex distribution for the pseudo-magnetic field can be generated. Furthermore, we performed tight-binding calculations of the local density of states (LDOS) by using the relaxed graphene configuration obtained from the atomistic calculations. We find that the quasiparticle LDOS are strongly modified near the pillars, both at low energies showing sub-lattice polarization, and at high energies showing shifts of the van Hove singularity. Our study shows that changing the specific pattern of the nano-pillars allows us to create a desired shape of the pseudo-magnetic field profile while the LDOS maps provide an input for experimental verifications by scanning tunneling microscopy.

Graphene is a newly discovered atomic thin two-dimensional honeycomb lattice consisting of carbon atoms¹. It is a zero gap semimetal with a conical band structure where the conduction and valence bands touch each other at the Dirac point². Nano-engineered non-uniform strain distribution in graphene is a promising road to generate a band gap and a pseudo-magnetic field. Scanning tunneling microscopy (STM) measurements have shown strain-induced Landau levels⁴ which correspond to a large pseudo-magnetic field. Shear strain is essential and neither uniaxial nor isotropic strain produces a strong uniform pseudo-magnetic field³.

Graphene's highly responses to external forces resulting in mechanical deformations. Over the last few years there have been many efforts to control graphene's electronic properties by strain⁵⁻⁷. Elastic deformations create a pseudo-magnetic field which acts on graphene's massless charge carriers⁸⁻¹⁰. The resulting variation of the hopping energies can be viewed as an induced pseudo-magnetic field which enters in the Dirac equation. Engineering of the right topology of the induced pseudo-magnetic field provides symmetrical magnetic confinement which confines electrons in specific regions in space¹¹.

Recently, it was predicted that non-uniform strain may lead to a considerable energy gap and a large gauge field that effectively acts as a uniform magnetic field¹². Recently, Tomori *et al* used pillars made of a dielectric material (electron beam resist) which were placed on top of a substrate which is then overlayed with graphene to generate non-uniform strain on a micro-scale¹³. The graphene sections which are located between the pillars are attached to the substrate and the size and separation of the pillars control the strength and distribution of the strain. The length scale in the experiment was micrometers and SiO₂ was used as the substrate¹³.

Here we study non-uniform strain at the atomistic scale where the continuum approach is no longer applicable. We also study the local density of state (LDOS) maps using the relaxed graphene configuration as input

for tight-binding calculations. We find very strong non-uniform pseudo-magnetic fields that can be created by depositing graphene on a substrate decorated with nano-scale pillars and find that the quasiparticle LDOS are strongly modified near the pillars. The optimum configuration of graphene over such nano-pillars depends on the imposed boundary conditions. The induced pseudo-magnetic fields are larger than 1000 Tesla and are spatially distributed around the nano-pillars. Decreasing the distance between the nano-pillars alters the six-fold symmetry of the pseudo-magnetic field distribution and results in a new configuration of magnetic confinement for the charge carriers on the graphene around the nano-pillars. Our study shows the LDOS maps around the pillars, which can be experimentally verified by STM.

Atomistic model. Classical atomistic molecular dynamics simulation (MD) is employed to find the optimum configuration of large flakes of graphene (GE) over the nano-pillars. The second generation of Brenner's bond-order potential is employed and is able to describe covalent sp³ bond breaking and the formation of associated changes in atomic hybridization within a classical potential¹⁴. The van der Waals (vdW) interaction between GE and nano-pillars/substrate is modeled by employing the Lennard-Jones (LJ) potential¹⁵⁻¹⁸.

In order to model the substrate, a (100) surface with lattice parameter equal to $\ell=3\text{ \AA}$ is assumed with LJ parameters σ_S and ϵ_S . The density of the sites in the substrate is $\Sigma_S = \ell^{-2}$ and the number of atoms is 13700. Nano-pillars are double-wall armchair carbon nanotubes (DWCNT) taken with (3,3) and (6,6) indexes including 144 atoms (see left insets in Fig 1). The number of atoms in the graphene sheet is 44800 which is equivalent to a sheet of size $34.8 \times 34.43 \text{ nm}^2$. We assume that both the substrate and nano-pillar atoms are rigid during the simulation.

To model the interaction between two different types of atoms such as carbon atom (C) and substrate atom (S), we adjust the LJ parameters using the equations $\epsilon_T = \sqrt{\epsilon_C \epsilon_S}$ and $\sigma_T = (\sigma_C + \sigma_S)/2$. The parameters for

carbon are $\sigma_C = 3.369 \text{ \AA}$ and $\epsilon_C = 2.63 \text{ meV}$. For the substrate atoms we took $\sigma_S = 3.5 \text{ \AA}$ and $\epsilon_S = 10.0 \text{ meV}$ which are typical for insulators, e.g. SiO_2^{15} .

The atomic stress experienced by each i^{th} atom can be expressed as^{19,20}

$$\eta_{\mu\nu}^i = \frac{1}{\Omega} \left(\frac{1}{2} m v_\mu^i v_\nu^i + \sum_{j \neq i} r_{ij}^\nu F_{ij}^\mu \right), \quad (1)$$

where the inner summation is over all the carbon atoms which are neighbors of the i^{th} atom which occupies a volume $\Omega = 4\pi a_0^3/3$. The quantities m and v^i denote the mass and velocity of i^{th} atom and the scalar r_{ij}^ν is the ν component of the distance between atoms 'i' and 'j'. F_{ij}^μ is the force on i^{th} atom due to atom j^{th} in the μ direction. We used this expression to calculate the stress on each atom. In order to be able to visualize the stress distribution on the GE atoms, we colored the atoms using a dimensionless invariant quantity²¹ $J_2 = \frac{1}{6}[(\eta_{xx} - \eta_{yy})^2 + (\eta_{yy} - \eta_{zz})^2 + (\eta_{zz} - \eta_{xx})^2 + 6(\eta_{xy}^2 + \eta_{xz}^2 + \eta_{yz}^2)]$, i.e. dark green (white) is related to a minimum (maximum) value of J_2 .

Strain induced pseudo-magnetic field. Coupling the Dirac equation, which governs the low energy electronics of graphene, to the curved surface is a common way to study the effects of graphene's curved geometries on its corresponding electronic properties^{9,10}. The metric of the curved surface describes the curvature of the surface. The origin of the deformations are external stresses that deform graphene so that the nearest neighbor distances become non-equal. The latter results in modified hopping parameters, which are now a function of the atomic positions $t(\mathbf{r})^{11}$. Assuming small atomic displacements ($\mathbf{u} = \mathbf{r}'_i - \mathbf{r}_i < a_0$) and rewriting the Dirac Hamiltonian in the effective mass approximation with non-equal hopping parameters yields the induced gauge fields:

$$\mathbf{A} = \frac{2\beta\hbar}{3a_0e}(u_{xx} - u_{yy}, -2u_{xy}), \quad (2)$$

where $\beta \sim 3$ is a constant and $u_{\alpha\beta}$ is the strain tensor including out of plane displacements⁹. The corresponding pseudo-magnetic field perpendicular to the $x - y$ plane is obtained as

$$B = \partial_y A_x - \partial_x A_y. \quad (3)$$

This is the pseudo-magnetic field that an electron experiences in the K-valley. We will find B by making the necessary differentiations numerically in the case of supported boundary conditions. Here we found that the major contribution is due to the out-of-plane terms, which appear mainly around the deformed parts. The other in-plane terms contribute less to the pseudo-magnetic field around the deformed parts particularly when the system is large as compared to the deformed regions.

Tight binding model The electronic properties are described by a tight-binding Hamiltonian for the π carbon orbitals. The minimal Hamiltonian, which describes

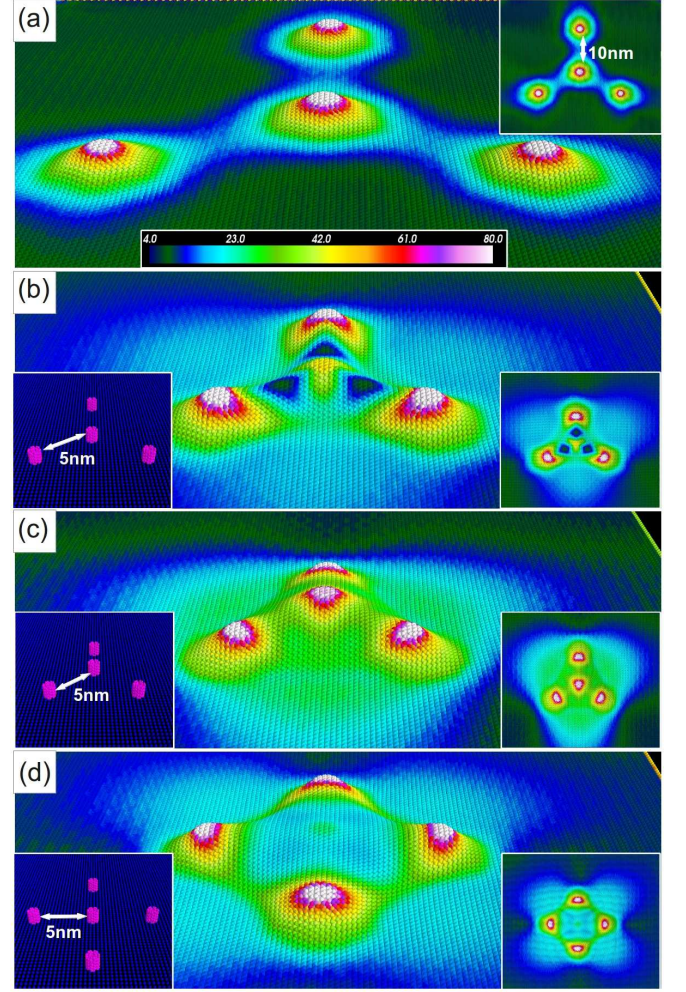


FIG. 1: (Color online) The optimal configuration of graphene on top of double wall armchair carbon nanotubes (nano-pillars) and a square lattice substrate (right-insets shows a top view). The left-insets show the nano-pillars and the substrate. In (a) the distance between pillars is 10 nm while in (c-d) it is 5 nm. All pillars are at the same height except (c) where the central pillar is 2 nm higher. Colors indicate the scaled stress distribution, i.e. white represents highest stress and dark-green lowest stress.

the low-energy band structure is:

$$\mathcal{H} = \sum_{\langle i,j \rangle, \sigma} -t(r_{ij}) c_{i\sigma}^\dagger c_{j\sigma} + h.c. \quad (4)$$

where $c_{i\sigma}^\dagger$ ($c_{j\sigma}$) creates (destroys) an electron at site i (j). The sum runs over nearest neighbors pertaining to opposite sub-lattices $\langle i, j \rangle$ and the electron spin, σ . In the following we will ignore the spin degrees of freedom since no spin-flipping term is present in the Hamiltonian.

The strain is included in the modified hopping amplitudes between π orbitals, $t_\pi(r_{ij})$, according to the empirical relation $t_\pi(r_{ij}) = \gamma_0 \exp^{3.37(\frac{r_{ij}}{a_0} - 1)}$, where $\gamma_0 = 2.7 \text{ eV}$ and $a_0 = 1.42 \text{ \AA}$ is the equilibrium inter-carbon distance⁵.

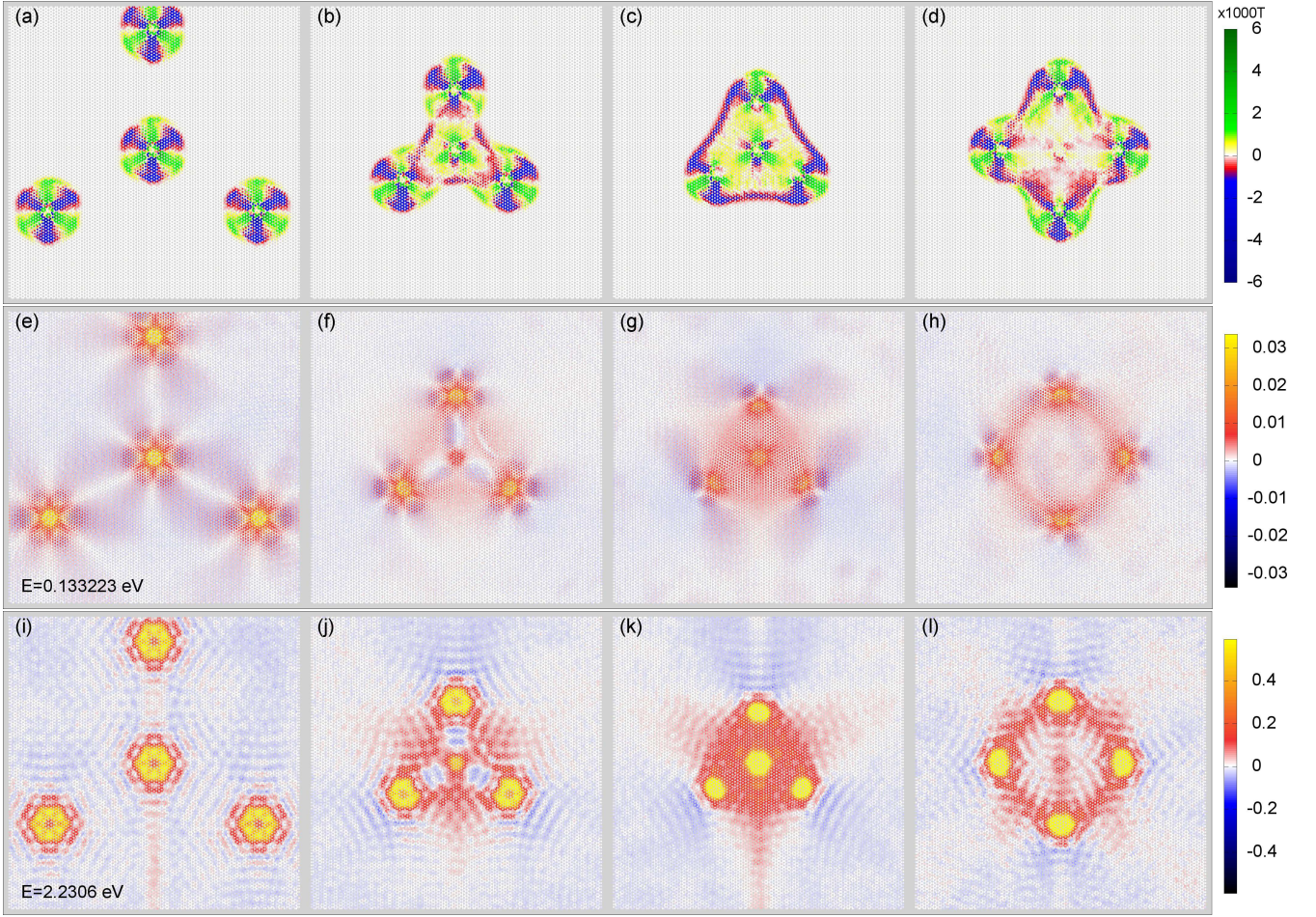


FIG. 2: (Color Online). (a-d) Pseudo-magnetic fields in one Dirac cone for 4 different pillar configurations shown in Fig. 1, respectively. (e-h) Low energy ($E=0.1332\text{eV}$) LDOS map and (i-l) high energy ($E=2.2306\text{eV}$) LDOS map for the same 4 configurations. Note that the bulk unstrained LDOS is subtracted from the LDOS maps.

This also gives a good approximation for the next-nearest neighbor hopping amplitude. We also consider the effect of misalignment of the π orbitals due to the finite curvature. This effect translates into the mixing of the π and σ orbitals. Depending on the local curvature, the modified hopping amplitude is:

$$t(r_{ij}) = t_\pi \sin(\theta_i) \sin(\theta_j) \cos(\phi) - t_\sigma \cos(\theta_i) \cos(\theta_j), \quad (5)$$

where θ_i and θ_j are the angles formed by the normals at each atom, \mathbf{n}_i and \mathbf{n}_j , with the inter-atomic distance \mathbf{r}_{ij} and ϕ describes the angle formed by the normal \mathbf{n}_j and the plane defined by \mathbf{n}_i and \mathbf{r}_{ij} ^{22–24}. The strain configuration and the curvature are extracted from the relaxed position of the graphene sheet obtained from our molecular dynamics simulation. For the systems considered here the effect of curvature is small when compared to the effect of strain on the hopping amplitudes.

Since the strain is inhomogeneous it is not possible to use any symmetries in the calculations of the electronic properties. Therefore, the system size considered here (44800 carbon atoms) becomes prohibitively large for an

exact digitalization of the Hamiltonian. Instead we will numerically obtain an approximation of the Green's function by using a Chebyshev expansion within the Kernel Polynomial method^{25–28}. The Green's function is defined as:

$$G_{ij}(\omega) = \langle c_i | \hat{G}(\omega) | c_j^\dagger \rangle \quad (6)$$

where $\hat{G}(\omega + i\eta) = [\omega + i\eta - \mathcal{H}]^{-1}$.

First a scaling of the excitation energies is performed, e.g. $\tilde{\mathcal{H}} = (\mathcal{H} - \mathbb{1}b)/a$, $\tilde{\omega} = (\omega - b)/a$ where $a = (E_{max} - E_{min})/(2 - \eta)$ and $b = (E_{max} + E_{min})/2$, where $\eta > 0$ is a small number. Following Refs. [25,27], the Green's function's components can be expressed as an expansion written in terms of Chebyshev polynomials:

$$G_{ij}(\tilde{\omega}) = \frac{-2i}{\sqrt{1 - \tilde{\omega}^2}} \sum_{n=0}^{\infty} a_n(i, j) e^{-i n \cdot \arccos(\tilde{\omega})} \quad (7)$$

where the coefficients $a_n(i, j) = \langle c_i | v_n \rangle$ can be obtained by an iterative procedure involving repeated applications

of the Hamiltonian on iterative vectors $|v_n\rangle$:

$$|v_{n+1}\rangle = 2\mathcal{H}|v_n\rangle - |v_{n-1}\rangle, \quad (8)$$

where $|v_0\rangle = |c_j^\dagger\rangle$ and $|v_{-1}\rangle = 0$. Significant computational speed-up is achieved when the computations are done on graphical processing units (GPU), i.e. video cards. The computations are performed on Nvidia GeForce GTX 580 cards.

The physical properties that can be straightforwardly extracted from the Green's functions are the local density of states (LDOS):

$$N_i(\omega) = -\frac{2}{\pi} \text{Im}[G_{ii}(\omega)], \quad (9)$$

the factor of 2 appears due to the summation over the spin components.

Results and discussion. At the start of our simulation we put graphene on top of the nano-pillars at $h_0 = 1.4\text{nm}$. The substrate is at zero height and the nano-pillars are located between graphene and the substrate. We have investigated two particular patterns of nano-pillars: i) five DWCNTs which have in-plane coordinates $(0,0)$ and $(\pm d, \pm d)$ with $d = 5, 10\text{nm}$, and ii) four DWCNTs at $(0,0)$, $(\pm d\sqrt{3}/2, \pm d/2)$ and $(0, -d)$. The height of DWCNTs was set to be 1nm (except in Fig. 1(c) which is 1.5nm). In order to prevent crumpling at the boundaries we only allow the boundary atoms to vibrate in the z -direction.

In Fig. 1 we show the optimal configuration of GE on top of four (a-c) and five (d) DWCNTs. Right insets in Figs. 1(a-d) show a top view. Notice that the stress distribution is mainly concentrated around the nano-pillars as expected. For the configuration presented in Fig. 1(a) the pillars are 10nm apart. Due to the vdW interaction the graphene sheet will stick to the substrate except around the pillars where the shape is close to a Gaussian even though deviations from an isotropic description exists. In the atomic limit, a slight anisotropy appears, the graphene sheet bends mostly in the zig-zag direction making the shape of the deformation hexagonal. In Figs. 1(b-d) the pillars are closer together (i.e. 5nm). Due to its large bending rigidity, the graphene sheet will be suspended over the substrate in the regions between the pillars. Depending on the pillar configuration, various stain configurations are achieved. If all the pillars have the same height, Figs. 1(b) and 1(d), most of the stress is obtained at the pillar location and where graphene sticks to the substrate. If one of the pillars is higher, Figs. 1(c), besides the maximal stress at the pillar location, high stress is also obtained throughout the suspended sheet.

The corresponding pseudo magnetic field profiles generated by the strain configurations are shown in Figs. 2(a-d). When the deformations are isolated, Fig. 2(a), the gauge field and the pseudo magnetic field exhibit six fold symmetry^{3,11} similar to a Gaussian deformation, $h(x,y) = G \exp(-\frac{x^2+y^2}{2\sigma^2})$. The continuum theory predicts that the pseudo-magnetic gauge field is

$\mathbf{A} = \frac{h(x,y)^2}{2\sigma^4}(x^2 - y^2, -xy)$ and the pseudo-magnetic field is $B = \frac{h(x,y)^2}{\sigma^6}(x^2 + y^2)\sin(3\theta)$, where θ is the azimuthal angle. Large pseudo-magnetic fields on the order of thousands of Teslas are obtained. When the graphene sheet is suspended, Figs. 2(b-d), the six-fold symmetry survives near the pillars but more complex pseudo-magnetic field profiles can be obtained, from large fields throughout the suspended sheet, Fig. 2(c), to fields localized only near the edges of the suspended sheet, Fig. 2(d). As seen from Figs. 2(c,d) the closer the pillars, triangular and rectangular magnetic field profile is created within the position of the pillars. In Figs. 2(c) there is a high magnetic field region at the center and the electron can not pass through this region.

In order to investigate the effect of the strain on the electronic properties, we input the relaxed positions of the atoms obtained from the atomistic simulation into the tight-binding model in order to find the LDOS maps around the pillars. These are shown in Figs. 2(e-h) for $E = 0.1332\text{eV}$ and in Figs. 2(i-l) for $E = 2.2306\text{eV}$. Two regimes can be observed, depending on the energy. For low energies, the pseudo-magnetic field will induce sub-lattice polarized states localized either near the pillars, Fig. 2(e), or in the regions with large pseudo-magnetic fields, Fig. 2(g). In the five-pillar configuration, Fig. 2(h), these low energy states are mostly localized near the edges of the suspended region. Interference patterns which depend on the energy are observed²⁹. A very different effect, which is not described by the low energy Dirac approximation³, is related to the shift of the van Hove singularity seen in unstrained graphene at $E = \gamma_0 = 2.7\text{eV}$. Because of strain, the hopping parameters will be modified, therefore locally shifting the van Hove singularity. This is observed in Figs. 2(i-l), where the enhancement of the LDOS is correlated with the stress and is enhanced where the stress is larger. Additional interference patterns appear between the pillars. The deviation from the Gaussian shape of the LDOS modification, i.e. the hexagonal shape, of the isolated deformations is also obvious from Fig. 2(i).

Conclusions. By combining molecular dynamics simulations with tight binding calculations we have shown how strain can be manipulated at the nano-scale. Isolated pillars show a six-fold symmetric pseudo-magnetic field and LDOS modification. By decreasing the distance between the pillars, the six fold symmetry of the pseudo-magnetic field is altered and a complex field profile appears within the suspended area. We found that by modifying the inter-pillar distances and the pillar heights one can design a particular desired magnetic field profile. Modifications of the hopping parameters due to changes in the C-C distances induced by strain, modify the LDOS around the deformations of the graphene sheet. Verifications of the six-fold symmetry of the LDOS near pillars could be easily confirmed with STM experiments.

Acknowledgment. This work was supported by the Flemish Science Foundation (FWO-VI) and the Euro-

-
- ¹ K. S. Novoselov *et al.*, Science **306**, 666 (2004).
 - ² A. H. Castro Neto *et al.*, Rev. Mod. Phys. **81**, 109 (2009).
 - ³ F. Guinea *et al.*, Nature Physics **6**, 30 (2010).
 - ⁴ N. Levy *et al.*, Science **329**, 544 (2010).
 - ⁵ Vitor M. Pereira *et al.*, Phys. Rev. B **80**, 045401 (2009).
 - ⁶ Z. Ni *et al.*, ACS Nano **3**, 483 (2009).
 - ⁷ T. M. G. Mohiuddin *et al.*, Phys. Rev. B **79**, 205433 (2009).
 - ⁸ F. Guinea *et al.*, Nature Physics **6**, 30 (2010).
 - ⁹ H. Castro Neto *et al.*, Rev. Mod. Phys. **81**, 109 (2009).
 - ¹⁰ F. Guinea *et al.*, Phys. Rev. B **77**, 075422 (2008).
 - ¹¹ K-J Kim *et al.*, Phys. Rev. B, **84**, 0814401(R) (2011).
 - ¹² S. Philip *et al.*, Appl. Phys. Lett. **94**, 032101 (2009).
 - ¹³ H. Tomoriet *et al.*, Applied Physics Express **4**, 075102 (2011).
 - ¹⁴ D. W. Brenner *et al.*, J. Phys.: Condens. Matter **14**, 783 (2002).
 - ¹⁵ Zhun-Yong Ong and Eric Pop, Phys. Rev. B **81**, 155408 (2010).
 - ¹⁶ M. Neek-Amal *et al.* Phys. Rev. E, **82** 051605 (2010).
 - ¹⁷ M. Neek-Amal and F. M. Peeters, Phys. Rev. B **81**, 235421 (2010).
 - ¹⁸ A. I. Zhbanov *et al.*, ACS Nano, **4**, 5937 (2010).
 - ¹⁹ N. Chandra *et al.*, Phys. Rev. B. **69**, 094101 (2004).
 - ²⁰ Q. X. Pei *et al.*, Carbon **48**, 898 (2010).
 - ²¹ H. Rafii-Tabar, Physics Reports **390**, 235 (2004).
 - ²² J. W. Klos *et al.*, Phys. Rev. B **80**, 245432 (2009).
 - ²³ S. Costamagna, O. Hernandez, and A. Dobry, Phys. Rev. B **81**, 115421 (2010).
 - ²⁴ M. J. Schmidt and D. Loss, Phys. Rev. B **81**, 165439 (2010).
 - ²⁵ A. Weisse *et al.*, Rev. Mod. Phys. **78**, 275 (2006).
 - ²⁶ G. Schubert and H. Fehske, Phys. Rev. Lett. **108**, 066402 (2012).
 - ²⁷ L. Covaci, F. M. Peeters, and M. Berciu, Phys. Rev. Lett. **105**, 167006 (2010).
 - ²⁸ L. Covaci and F.M. Peeters, Phys. Rev. B **84**, 241401(R) (2011).
 - ²⁹ A movie of the LDOS maps for different energies is provided in the Supplementary Material.